Am J Cancer Res 2012;2(5):581-588
www.ajcr.us /ISSN:2156-6976/ajcr0000138

Original Article

Vascular development in mouse lung metastases

Howard W Salmon[1], Ananya Guha[2], Amyn M Rojiani[3], Dietmar W Siemann[4]

[1]North Florida Radiation Oncology, North Florida Regional Medical Center, Gainesville, FL, USA; [2]College of Medicine, University of Florida, Gainesville, Florida, USA; [3]Department of Pathology, GHSU-Medical College of Georgia, Augusta, Georgia, USA; [4]Department of Radiation Oncology, College of Medicine, University of Florida ,Shands Cancer Center, Gainesville, Florida, USA

Received July 23, 2012; accepted August 10, 2012; Epub August 20, 2012; Published September 15, 2012

Abstract: Dissemination of cancer cells is strongly associated with reduction in quality of life, worsening of prognosis, and remains the primary cause of therapeutic failure and high mortality in cancer. A crucial factor in the progression of metastases is the ability to establish a functioning blood vessel network. Consequently therapeutic strategies which selectively target tumor vasculature may hold promise for the treatment of metastatic disease. A complicating factor in the assessment of the efficacy of vascular targeting therapies is that the metastatic process can result in multiple neoplastic lesions at various stages of growth and vascularity in a single organ. The goal of this project was to utilize a rodent squamous cell carcinoma (SCCVII) model to characterize the development of metastatic lung lesions and their associated vasculature. Mice were injected with tumor cells via the tail vein to introduce a reproducible number of lung metastases. At various times after cell injection, lungs were removed and serial sections were taken throughout the lobes for morphometric analysis. Tumor volumes were calculated for each nodule using 2 hematoxylin and eosin (H&E) stained sections that were a known distance apart. Sections adjacent to those used for size determination were reserved for immunohistochemical staining with CD31 to identify blood vessels associated with each nodule. The results showed that although the median tumor volume increased from 0.006 to 0.51 mm^3 between 7 and 18 days post SCCVII cell injection, a range of tumor sizes existed at all-times. Irrespective of the time of assessment, nodules with volumes $\leq$ 0.5 mm^3 had a constant vessel density while those with volumes >0.5 mm^3 showed increasing vessel densities with increasing size. These findings indicate that the methodology outlined in this study can identify metastases in various stages of vascular development and could therefore be applied to evaluate and distinguish therapeutic interventions that seek to prevent the initiation of blood vessel networks and those targeting already established expanding tumor vasculature. Examining the efficacy of such approaches, alone or in combination, in the treatment of metastases in a preclinical model could lead to the development of more effective therapeutic strategies for metastatic disease.

Keywords: Metastasis, vascular development, carcinoma

Introduction

Despite improvement in early detection, more refined diagnostic modalities, and a better understanding of the natural history of cancer, metastatic disease remains the primary reason for treatment failures responsible for the majority of cancer deaths [1-3]. Metastasis is the spread of malignant cells from a primary tumor, leading to the establishment of secondary tumors at a distant site. The metastatic cascade involves a series of sequential steps which a tumor cell must perform to establish a secondary growth. These include leaving the primary tumor, surviving in the harsh environment of the bloodstream, evading host immune surveillance, escaping the circulation, establishing metastatic growth, and attracting an independent blood supply [4, 5]. Given the complexity of the process, even when injected directly into the blood stream in experimental settings only ~0.1 to 1% of tumor cells produce metastases [6]. Still, roughly two-thirds of cancer patients suffer from metastases during their life time [1, 2].

The critical role of metastasis in cancer patient prognosis and management has led to investigations of the process both in vitro and in vivo. In vitro assays enable the detailed study of some of a tumor cell's ability to perform a single step in the multi-step metastatic cascade in depth, while animal models allow the analysis of

the metastatic process as a whole [7]. Thus, researchers have developed animal models to analyze the metastatic phenotype of tumor cells and evaluate the efficacy of anti-cancer agents. These metastasis models include the chick embryo metastasis model, transgenic animal models, xenograft models in SCID or nude mice, and syngeneic murine tumor models [7]. Typically, xenograft models have a low and highly variable rate of metastasis in comparison to syngeneic models, which readily develop metastases in a predictable manner [7, 8].

A key factor in establishing successful metastatic growth at a secondary site is the ability of tumor cells to initiate angiogenesis. Indeed it has been long recognized that when tumors are avascular, the diffusion of nutrients and waste products limit their growth and for further progression tumors must develop their own network of microvessels through the process of neovascularization [9]. The critical role of vasculature in tumor development and the unique features of tumor blood vessels have led researchers to explore treatment strategies which selectively target tumor vasculature [3, 10-13]. Vascular targeting strategies encompass 2 approaches: interventions which interfere with new blood vessel formation, anti-angiogenic agents, and therapies which target existing neovasculature in expanding tumors, vascular disrupting agents [14]. While these types of therapeutic approaches are being extensively studied in primary tumor response evaluations in the clinic, it is clear that they may have particular utility in the treatment of metastatic disease. The goal of the present investigations was to quantify the vascular development of multiple metastatic lesions growing simultaneously in the lungs. Since at a given point in time different metastatic lesions can concurrently exist in various stages of vascular development and vascular targeting agent efficacy is dependent on the nature of the vasculature at the time of treatment, such studies provide important insights for future blood vessel directed targeting approaches designed to inhibit metastasis.

Materials and methods

Animal and tumor models

Female 6 to 8 week-old C3H/HeJ mice (Jackson Laboratories: Bar Harbor, Maine), were maintained under specific-pathogen-free conditions at the University of Florida Health Science Center with food and water supplied ad libitum. SCCVII murine squamous cell carcinoma cells were passaged in vitro in α-MEM medium containing penicillin/streptomycin and 10% fetal bovine serum and incubated in 5% CO_2 and air at 37°C.

Experimental lung metastasis

To initiate lung metastasis, $1x10^4$ SCCVII cells suspended in 20 μl 0.9% saline were injected into the lateral tail vein of C3H/HeJ mice. Experiments consisted of 12 mice inoculated with tumor cells on day 0. After cell injection, mice were randomly sorted into experimental groups to be assessed 7, 10, 14 and 18 days later. All research was governed by the principles of the Guide for the Care and Use of Laboratory Animals and approved by the University of Florida Institutional Animal Care and Use Committee.

Lung tissue preparation

Mice were killed by CO_2 asphyxiation followed by cervical dislocation (as approved by the University of Florida Institutional Animal Care and Use Committee) and the lungs were removed and dissected from other mediastinal structures. Lungs were rinsed in phosphate buffered saline to remove blood and then fixed in 4% paraformaldehyde for 2 hr. Tissues were embedded in paraffin and a sampling of sections were taken across each lung in the following manner. Two consecutive 4 μm sections were taken and then a number of consecutive 4 μm sections were discarded (typically 20 to 40 depending on the size of the lung tumor nodule) before collecting another two consecutive 4 μm sections (**Figure 1**). This process was repeated along the entire length of each lung lobe. The consecutive sections were then stained using Hematoxylin and Eosin (H&E) and CD31 respectively. For the latter, the primary CD31 antibody (BD Pharmingen) was diluted 1:10 and the sections were incubated at room temperature for 1 hr. The secondary mouse-absorbed biotinylated rabbit anti-rat antibody (Vector Labs) was incubated at room temperature for 30 min. Detection of the primary antibody was performed using the VIP Substrate Kit (Vector Labs) according to the manufacturer's protocol.

Imaging

H&E Paraffin sections were imaged at 5X magnification using a morphometric microscope

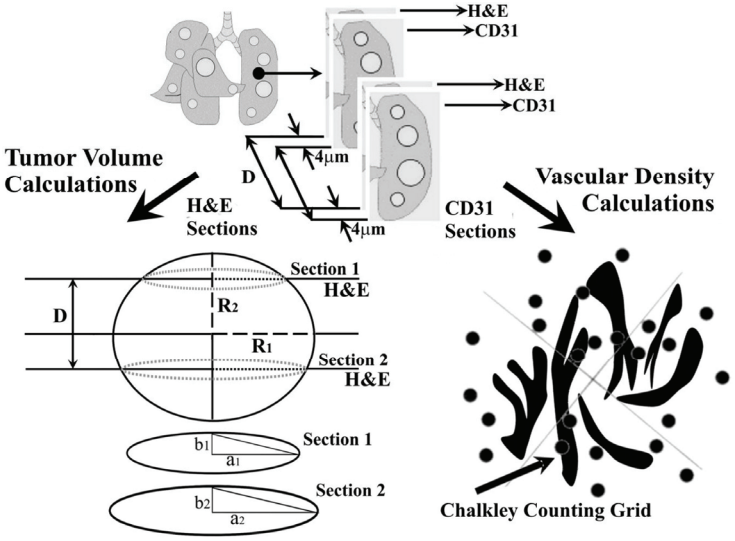

Figure 1. Schematic illustration showing the process by which tumor lung nodule volumes and vascular densities were determined.

(McKnight Brain Institute, University of Florida). This microscope was fitted with a motorized scanning stage capable of "tiled field mapping"; a function which allows the stitching together of several high resolution images into a single output image. To aid quantification each of the output images was fitted with a calibration scale. Once a lung nodule had been marked for evaluation (**Figure 2**), additional tile field map images were taken (40X magnification) of their matched CD31 labeled [15] paraffin sections (**Figure 5**).

Tumor volume quantification

Tumor volume was calculated using the adapted "Prolate Spheroid" model (**Figure 1**). This model allows the determination of the volume of any given lung tumor nodule, on the basis of measurements of the radii of two sections and known separation between the two sections

$$Tumor\ Volume = \left(4/3\right)\pi\, R_1\, R_2^{\,2} \qquad R_1 \geq R_2$$

$$R_1 = \left[\frac{\left(a_2^2 - a_1^2 + D^2\right)^2}{4\,D^2} + a_1^2\right]^{\frac{1}{2}}$$

$$R_2 = \left[\frac{\left(b_2^2 - b_1^2 + D^2\right)^2}{4\,D^2} + b_1^2\right]^{\frac{1}{2}} \qquad \text{Eq. 1}$$

$$\{Equation 1\}$$

as illustrated in **Figure 1**. Then by using **Equation 1**, the volume of each lung tumor nodule can be determined.

Vascular density measurements

The number of blood vessels was counted using a Chalkley point array [16] for random sample analysis [17]. Briefly, each section was viewed with a 25-point Chalkley grid (**Figure 1**) positioned over the field of view, and vascular density was recorded as the number of vessels per unit area as previously described [18].

Statistical analysis

The results were analyzed using ANOVA in combination with Scheffe's post-hoc procedure, and expressed as median ± standard deviation. Differences were considered statistically significant at $P < 0.05$.

Results

The growth and development of vasculature in experimental lung metastases was characterized in the SCCVII squamous cell carcinoma model. After direct injection into the bloodstream via the lateral tail vein, tumor cells arrest in the pulmonary capillaries, extravasate, multiply, and initiate neovasculature. This study used immunohistochemistry to characterize both SCCVII tumor lung nodule development as well as tumor vasculature induction. On various days after intravenous tumor cell injection, lungs were removed and sections taken for morphometric analysis as illustrated schematically in **Figure 1**.

Initial experiments were designed to establish the variation in tumor lung nodule size as a function of time. Measurements of two diameters of a lung tumor nodule visible on two H&E stained sections a known distance apart were made under a microscope. The volume of the tumor nodule was then calculated using Equation 1. An example of two H&E stained sections that are 80 μm apart is shown in **Figure 2**. Only nodules 1-4 are apparent on both sections allowing volume determinations of these four

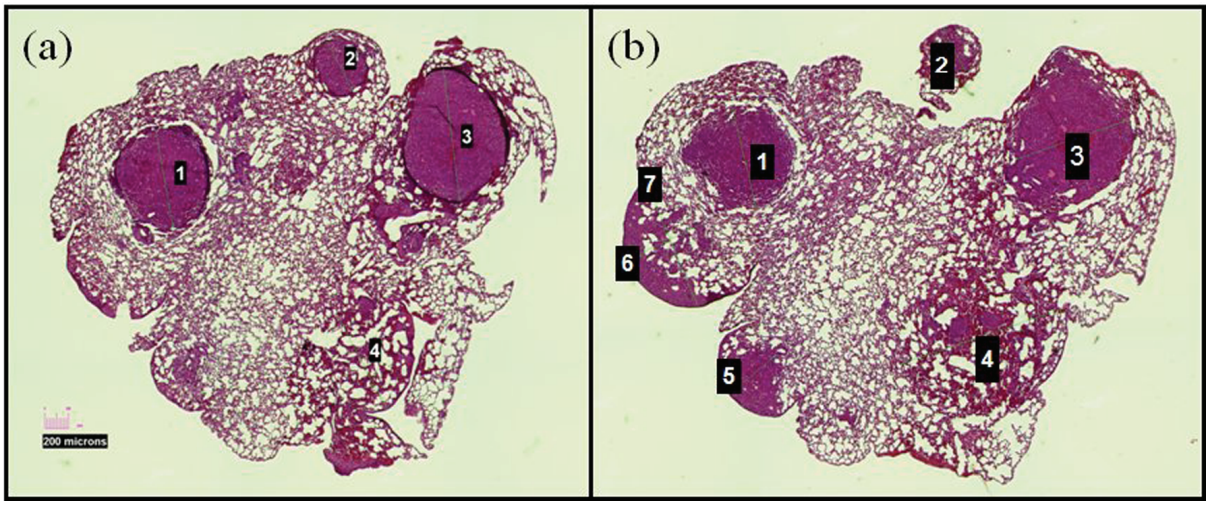

Figure 2. Example of two H&E sections taken 80 μm apart. Colonies 1-4 are readily apparent on both sections and volumes could be calculated according to Equation 1.

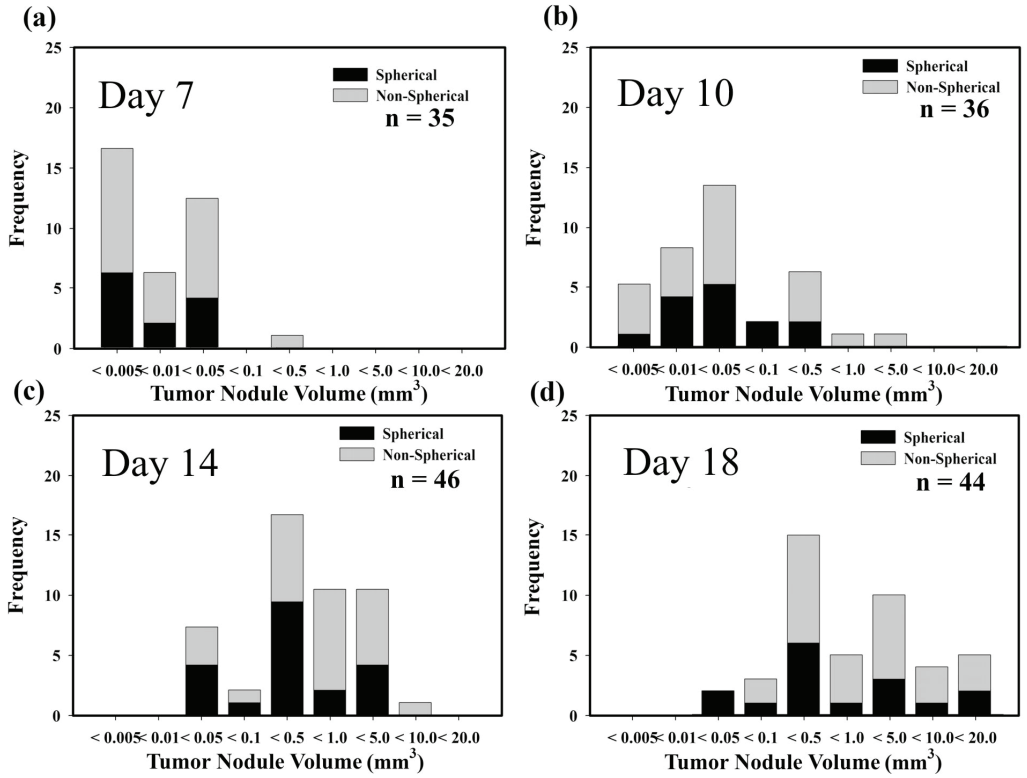

Figure 3. Distribution plots showing the variation in SCCVII tumor nodule volume as a function of time after intravenous injection of tumor cells.

nodules to be made.

Figure 3 shows the distribution in nodule sizes on days 7, 10, 14 and 18 after intravenous tumor cell inoculation. Since less than half of the tumor nodules measured were spherical in shape, the nodule size data were also subdivided in terms of tumor nodule shape. For this

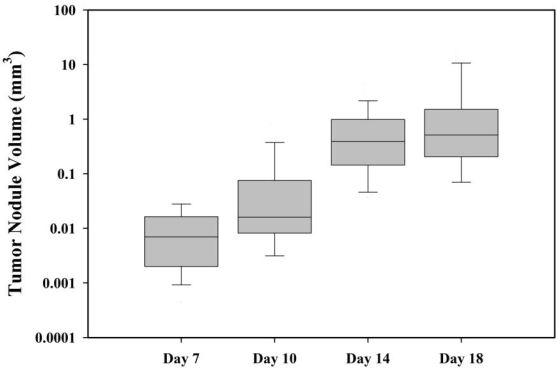

Figure 4. Box plot showing the median SCCVII tumor nodule volume as a function of time after tumor cell injection. Data represent the median of 33 to 46 tumors nodules (bar), 25-75% confidence interval (box), and 10-90 % confidence intervals (whiskers).

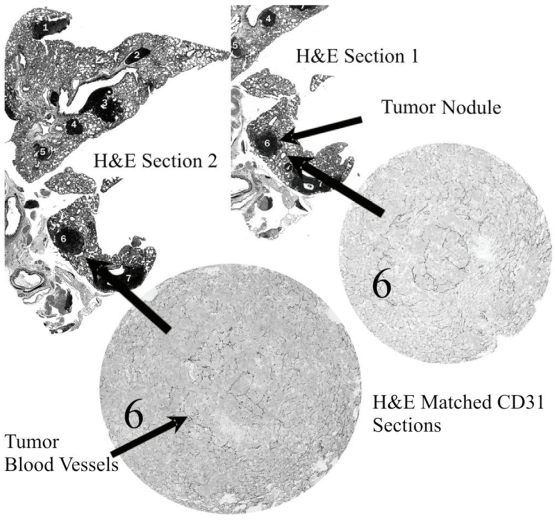

Figure 5. Example H&E and CD31 labeled sections, showing SCCVII tumor nodules within the mouse lung.

analysis, any tumor nodule that showed a greater than 20% variation within the measured values of "a1, a2, b1, b2" (**Figure 1**), was classified as non-spherical in shape. The volumes of spherical and non-spherical nodules are shown in the four panels of **Figure 3** as black and shaded bars respectively. The volumes of both types of lung nodules readily increased as a function of time but Anova analysis revealed no statistical significance between the groups of spherical or non-spherical nodules at any of the days investigated. Consequently volumes of all SCCVII lung nodules were pooled in the growth analysis as a function of time shown in **Figure 4**. The results indicate that median tumor volume increases from 0.006 mm^3 on day 7 to 0.016 mm^3 on day 10 and 0.39 and 0.51 mm^3 on days 14 and 18, respectively.

To investigate the vascular development in growing SCCVII lung nodules the blood vessel density within these tumor lung nodules was determined using the Chalkley counting technique [16, 18]. Endothelial cell labeled sections matched to the adjacent H&E stained sections used to measure nodule volumes (**Figures 2** and **5**) were scored. The results (**Figure 6A**) showed little change in tumor nodule vessel density (3-4 hits per unit area) for tumor nodule sizes ranging from smallest detectable to ≤ 0.5 mm^3. However, as the lung nodules grew larger (>0.5 mm^3) a steady increase in nodule vasculature was noted. The vessel density data were also subdivided into spherical and non-spherical tumor nodules. As was the case for the tumor growth assessment (**Figure 3**), the results showed no statistical difference between the vascular development in spherical and non-spherical SCCVII lung nodules (**Figure 6B**).

Discussion

Metastasis is the major cause of therapeutic failure in cancer patients. A common site of metastases in humans is the lungs [19, 20]. In general, lung metastasis signifies widespread cancer with a poor survival rate, and living more than 5 years with metastatic cancer to the lungs is rare [20]. Clearly, there is a need for therapeutics that combat metastatic cancer to the lungs and have low toxicity in normal tissues. One area of anticancer drug development that has received considerable attention over the past 2 decades is focused on targeting tumor angiogenesis and the unique features of tumor vasculature [5, 11, 13]. Cancer cell survival, growth, and opportunity for metastasis depend on a tumor's ability to attract and maintain a functional blood supply [21]. In primary tumors, damaging the endothelium may impact a large number of cancer cells. Based on the observation that oxygen can diffuse a distance of ~100 to 150 μm, it is estimated that 10,000 malignant cells may be sustained for every millimeter of capillary growth in tumor angiogenesis [21]. Furthermore, the irregularities in tumor microenvironments caused by aberrant vasculature may

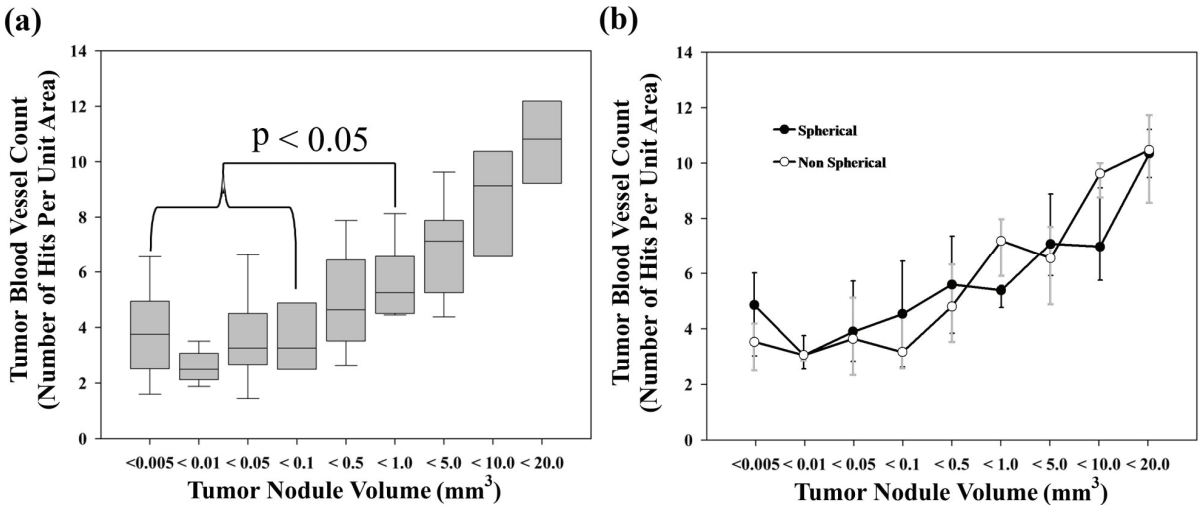

Figure 6. Vascular density as determined by Chalkley counting method; (A) shows the vascular density in all SCCVII tumor lung nodules as a function of lung tumor nodule size (n = 156); data represent the median of 35 to 46 tumors nodules (bar), 25-75% confidence interval (box) and 10-90% confidence interval (whiskers); (B) change in SCCVII vascular density as a function of nodule shape and volume (spherical n = 53; non-spherical n = 103). Data represent the median and 10-90% confidence interval.

render tumor cells more likely to metastasize [22]. Several reports have linked poor primary tumor oxygenation to development of metastases in soft tissue sarcoma, cervical carcinoma and squamous cell carcinoma of the head and neck [23-25]. When applied in the clinic, small but encouraging clinical benefits have been observed when blood vessel directed therapies are combined with chemotherapy and radiotherapy leading to the inclusion of such agents in first or second line therapy for some malignancies [26-28].

The focus of the present study was to investigate the growth and vascular development of squamous carcinoma cells seeding in the lungs. An experimental metastasis assay involving the injection of tumor cells directly into the bloodstream via the lateral tail vein was used. Though not including the entire metastatic cascade, the experimental lung metastasis model has several advantages. Because cells are directly injected into the bloodstream, control of the primary tumor is not necessary to evaluate the growth of metastases. By injecting a constant number of tumor cells, a predictable number of metastases are formed per animal. Even so when utilizing H&E stained sections to calculate lung tumor nodule volumes, from radii of sections separated by a known distance (**Figure 1**), it became readily apparent (**Figures 2** and **3**) that there exists considerable variability in the time of establishment and subsequent growth of these metastases.

Moreover not all tumor nodules were spherical in shape, raising the question of whether non-spherical tumor nodules grew at a different rate than did spherical ones. However, statistical analysis of these two subsets revealed this not to be the case. The pooled results of all measurements (**Figure 4**) show how the median volume of SCCVII lung tumor nodules increased from 0.006 mm^3 on day 7 to 0.51 mm^3 on day 18.

Sections adjacent to those used for nodule measurement (**Figures 1** and **5**) were reserved for immunohistochemical analysis using the endothelial cell marker CD31. This methodology allowed the direct association of tumor nodule size and vascular development irrespective of the evaluation time point; an important consideration given that nodule size varied considerably at a particular assessment time point (**Figure 4**). Vascular density determined using the previously described Chalkley counting technique [16, 18] showed that blood vessels were present in all tumor nodules even at the smallest detectable size (**Figure 6A**). However, closer examination of the data showed a consistent density of blood vessels in all SCCVII tumor nod-

ules of sizes ≤ 0.5 mm^3, while the vascular density found in nodules greater than 0.5 mm^3 increased with increasing nodule size. Again, as was the case for tumor growth (**Figure 3**), when the effects of tumor nodule shape were considered, no difference in vessel density was seen between nodules classified as spherical or non-spherical (**Figure 6B**).

The present investigation utilized immunohistochemical and H&E staining to simultaneously assess the vascular development of multiple SCCVII lung metastases at various stages of growth. Irrespective of the day of assessment, tumor deposits ranging from the smallest size detectable to ≤ 0.5 mm^3 always demonstrated similar blood vessel densities. This finding suggest that following blood borne dissemination, expanding SCCVII tumor cell populations are initially able to meet their nutritional and waste product removal needs by relying strictly on the preexisting lung vasculature, and tumor initiated blood vessel formation is not required. This is not however the case in larger metastases where increasingly greater blood vessel densities reflect an association between progressive tumor growth and additional vascular development. The induction of tumor vasculature first occurs in SCCVII lung metastases at a size of 0.5 to 1 mm^3 and is independent of tumor nodule shape. The observation that blood vessel induction begins to take place in tumor deposits < 1 mm^3 is consistent with prior window chamber tumor studies which reported that angiogenesis can be initiated by tumor cell numbers smaller than anticipated [29, 30].

In light of the importance of the vasculature to tumor cell survival and progression extensive efforts have been made to develop blood vessel directed therapies as anticancer treatments. Two fundamental treatment strategies have emerged [31]; those interfering with tumor associated initiation of new blood vessels (anti-angiogenic agents), and those targeting the established tumor blood vessel network (vascular disrupting agents). These two classes differ in three key respects: their physiologic target, the type or extent of disease that is likely to be susceptible, and the treatment scheduling [14]. Indeed preclinical investigations have already established early stage tumors to be more susceptible to angiogenesis inhibition and advanced disease to be more efficiently targeted by vascular disrupting agents [32, 33]. Since metastases can simultaneously exist in organs at various stages of development (dormant, early phases of growth, well-established macroscopic neoplastic lesions), they will not only present with a variety of vascular developments but as a consequence will also be susceptible to different blood vessel directed therapeutics. The present methodology offers the opportunity to simultaneously assess the response of multiple metastases at various stages of growth to treatments targeting the tumor blood vessel network. Such information would provide valuable insights into treatment regimens which specifically target the tumor vasculature and aid the determination of which therapeutic interventions used alone or in combination might have particular utility in a metastasis setting.

Acknowledgements

This work was supported by USPHS grant CA089655. The authors gratefully acknowledge the Optical Microscopy Facility, Evelyn F & William L McKnight Brain Institute of the University of Florida, Gainesville, Florida in the performance of these studies.

Address correspondence to: Dr. Dietmar W. Siemann, Department of Radiation Oncology, University of Florida, 2000 SW Archer Road, Gainesville, FL 32610, USA E-mail: siemadw@ufl.edu

References

[1] Coghlin C and Murray GI. Current and emerging concepts in tumour metastasis. J Pathol 2010; 222: 1-15.
[2] Wittekind C and Neid M. Cancer invasion and metastasis. Oncology 2005; 69 Suppl 1: 14-16.
[3] Sleeman J and Steeg PS. Cancer metastasis as a therapeutic target. Eur J Cancer 2010; 46: 1177-1180.
[4] Fidler IJ. Critical determinants of metastasis. Semin Cancer Biol 2002; 12: 89-96.
[5] Carmeliet P and Jain RK. Angiogenesis in cancer and other diseases. Nature 2000; 407: 249 -257.
[6] Luzzi KJ, MacDonald IC, Schmidt EE, Kerkvliet N, Morris VL, Chambers AF and Groom AC. Multistep nature of metastatic inefficiency: dormancy of solitary cells after successful extravasation and limited survival of early micrometastases. Am J Pathol 1998; 153: 865-873.
[7] Metastasis Research Protocols. Totowa, NJ: Humana Press, 2001.
[8] Khanna C and Hunter K. Modeling metastasis in vivo. Carcinogenesis 2005; 26: 513-523.
[9] Folkman J. How is blood vessel growth regu-

lated in normal and neoplastic tissue? G.H.A. Clowes memorial Award lecture. Cancer Res 1986; 46: 467-473.
[10] Randal J. Antiangiogenesis drugs target specific cancers, mechanisms. J Natl Cancer Inst 2000; 92: 520-522.
[11] Siemann DW, Chaplin DJ and Horsman MR. Vascular-targeting therapies for treatment of malignant disease. Cancer 2004; 100: 2491-2499.
[12] Siemann DW and Horsman MR. Vascular targeted therapies in oncology. Cell Tissue Res 2009; 335: 241-248.
[13] Hicklin DJ and Ellis LM. Role of the vascular endothelial growth factor pathway in tumor growth and angiogenesis. J Clin Oncol 2005; 23: 1011-1027.
[14] Siemann DW, Bibby MC, Dark GG, Dicker AP, Eskens FA, Horsman MR, Marme D and Lorusso PM. Differentiation and definition of vascular-targeted therapies. Clin Cancer Res 2005; 11: 416-420.
[15] Ilan N and Madri JA. PECAM-1: old friend, new partners. Curr Opin Cell Biol 2003; 15: 515-524.
[16] Chalkley HW. Methods for quantitative morphologic analysis of tissues. J Natl Cancer Inst 1943; 4: 47-53.
[17] Curtis AS. Area and volume measurements by random sampling methods. Med Biol Illus 1960; 10: 261-266.
[18] Salmon HW, Mladinich C and Siemann DW. Evaluations of the renal cell carcinoma model Caki-1 using a silicon based microvascular casting technique. Technol Cancer Res Treat 2006; 5: 45-51.
[19] Nguyen DX, Bos PD and Massague J. Metastasis: from dissemination to organ-specific colonization. Nat Rev Cancer 2009; 9: 274-284.
[20] Rusch VW. Lung metastases. In: Abeloff MD, Armitage JO, Niederhuber JE, Kastan MB, McKenna WG. Abeloff's Clinical Oncology. 4th ed. Philadelphia, Pa: Churchill Livingstone Elsevier; 2008: chap 58.
[21] Folkman J. The vascularization of tumors. Sci Am 1976; 234: 58-64, 70-53.
[22] De Jaeger K, Merlo FM, Kavanagh MC, Fyles AW, Hedley D and Hill RP. Heterogeneity of tumor oxygenation: relationship to tumor necrosis, tumor size, and metastasis. Int J Radiat Oncol Biol Phys 1998; 42: 717-721.
[23] Brizel DM, Schroeder T, Scher RL, Walenta S, Clough RW, Dewhirst MW and Mueller-Klieser W. Elevated tumor lactate concentrations predict for an increased risk of metastases in head -and-neck cancer. Int J Radiat Oncol Biol Phys 2001; 51: 349-353.
[24] Brizel DM, Scully SP, Harrelson JM, Layfield LJ, Bean JM, Prosnitz LR and Dewhirst MW. Tumor oxygenation predicts for the likelihood of distant metastases in human soft tissue sarcoma. Cancer Res 1996; 56: 941-943.
[25] Nordsmark M, Bentzen SM, Rudat V, Brizel D, Lartigau E, Stadler P, Becker A, Adam M, Molls M, Dunst J, Terris DJ and Overgaard J. Prognostic value of tumor oxygenation in 397 head and neck tumors after primary radiation therapy. An international multi-center study. Radiother Oncol 2005; 77: 18-24.
[26] Jain RK, Duda DG, Clark JW and Loeffler JS. Lessons from phase III clinical trials on anti-VEGF therapy for cancer. Nat Clin Pract Oncol 2006; 3: 24-40.
[27] Rock EP, Goodman V, Jiang JX, Mahjoob K, Verbois SL, Morse D, Dagher R, Justice R and Pazdur R. Food and Drug Administration drug approval summary: Sunitinib malate for the treatment of gastrointestinal stromal tumor and advanced renal cell carcinoma. Oncologist 2007; 12: 107-113.
[28] Harshman LC and Srinivas S. The bevacizumab experience in advanced renal cell carcinoma. Onco Targets Ther 2010; 3: 179-189.
[29] Li CY, Shan S, Huang Q, Braun RD, Lanzen J, Hu K, Lin P and Dewhirst MW. Initial stages of tumor cell-induced angiogenesis: evaluation via skin window chambers in rodent models. J Natl Cancer Inst 2000; 92: 143-147.
[30] Cao Y, Li CY, Moeller BJ, Yu D, Zhao Y, Dreher MR, Shan S and Dewhirst MW. Observation of incipient tumor angiogenesis that is independent of hypoxia and hypoxia inducible factor-1 activation. Cancer Res 2005; 65: 5498-5505.
[31] Siemann DW. The unique characteristics of tumor vasculature and preclinical evidence for its selective disruption by Tumor-Vascular Disrupting Agents. Cancer Treat Rev 2011; 37: 63-74.
[32] Gerber HP and Ferrara N. Pharmacology and pharmacodynamics of bevacizumab as monotherapy or in combination with cytotoxic therapy in preclinical studies. Cancer Res 2005; 65: 671-680.
[33] Siemann DW and Rojiani AM. The vascular disrupting agent ZD6126 shows increased antitumor efficacy and enhanced radiation response in large, advanced tumors. Int J Radiat Oncol Biol Phys 2005; 62: 846-853.